Precision Kinetic High-Resolution Analysis of DNA Damage Patterns

Anil Kumar

Bharati Vidyapeeth's College of Engineering, New Delhi – 110063 (India)

*Corresponding Author, Email: dranilchhikara@gmail.com

Abstract: 53BP1, a protein known to interact with p53, has been isolated in vitro, but its critical role in supporting the p53-driven transcriptional program in the DNA Damage Response (DDR) is often overlooked. This is evident even when assessing different reactions to DNA Double-Strand Breaks (DSBs) caused by ionizing radiation. Inhibiting 53BP1 is key to optimizing both mental and physical performance by easing their interaction. This study introduces advanced image cytometry to track DDR progression, highlighting 53BP1 translocation from damage sites where it regulates DDR. By analyzing cell cycle deficiencies, we provide a quantitative framework of molecular interactions and their spatial-temporal constraints. We offer a detailed quantitative analysis of the processes following DSBs, validated through rigorous testing. Using Single-Molecule Localization Microscopy (SMLM), we confirm the p53-53BP1 interaction at critical DDR stages, offering new insights into their coordination.

Keywords: 53BP1, p53fluorescence microscopy; image analysis; image cytometry, "DNA damage response;"

I. "Introduction"

DNA double-strand breaks (DSBs) are among the most perilous threats to genomic integrity. The DNA Damage Checkpoint Repair (DDR) apparatus, a convoluted sub-atomic connection used by cells to manage responses to DNA harm, played a starring role in allowing cells to detect and repair damage. Upon DSB testimony by the MRE11-Rad51-NBS1 (MRN) baffled, a hailing flood begins to continuously choose particles to repair the damage, triggering a cell cycle arrest and, if the DNA breaks are not mended, senescence or apotosis. There are two well-defined repair mechanisms for DSBs, and they are conventional Non-Homologous End-Joining (c-NHEJ) and Homology-Worked with Obsession (HDR). Considering its essential role in validating the DSB repair pathway, the p53 Limiting Protein 1 (53BP1) is likely to play a significant role in transmitting c-NHEJ. One other p53 DNA binding space interactor, ASPP2 (53BP2), was thought to be located close to 53BP1 all along. Although the cooperation between these proteins has been thoroughly considered, p53's role as a definitive regulator in determining cell-cycle progression and whether cells are affected by their persistent situation remains tenuous. 53BP1's important role in p53's standard of cell predetermination programmes has been highlighted in recent reviews. 53BP1 may potentially express spatially changing rehearses for DSBs foci and p53-committed genomic loci since the cell uses nuclear spatiotemporal relocalization to control and work with its cycles. To put the accepted correlation between intracellular region and criticality to the test, a large enough spatial frame is necessary. Structures groupings like Stochastic Optical Duplication Microscopy (Hurricane) and PhotoActivated Impediment Microscopy (PAIM), are capable of certifying single-cell iotas with a resolution of 200 n (PALM). In spite of this, considering the permanently constrained field of view, expanding the spatial aim is always accompanied by a decrease in the likelihood of the reliable evaluation. Numerically relaxing the brilliant lights to gather as many photons as possible for consideration is a crucial part of wide field fluorescence microscopy while still providing a practical field of vision. Unfortunately, this careful thinking and advancement towards object level were often employed to focus in on the development of the contained

particles. To address this, we included an image cytometry process into our strategy for robotized fluorescence microscopy. The evidence prompted displays and computational devices to ponder the provision of diffraction-bound imaging to a trustworthy sam pling in the reference to a few enormous numbers of cells. Furthermore, superior staining takes into account the structured evaluation of up to seven fluorescence channels, which reveals details that were previously hidden. Here, we used the developed tools to provide a quantitative description of the DNA Mischief Response (DDR) in cells that have been conditioned to X-clarification in order to better tolerate ionising radiation (IR). Using the "heartbeat and pursuit" display that is unique to stream cytometry, we solidified the voluminous testing and quality of a diffraction-bound evaluation. We then had the opportunity to provide a quantitative description of the varied effects DNA Naughtiness (DD) assurance has on distinct populations of cells, as shown by their relatively stable stages in the cell cycle. This kind of thought contributes to the perhaps further oversight of any potentially out-of-date components that may have been initiated by too synchronised, ill-suited structured subject matter experts. After the primary harvest, a 3D titanic standard picture gathering of express amounts of cash as seen by picture cytometry evaluation was repeated using the probability of recovering mind-blowing cells. Finally, we used District Ligation Assessment (PLA) and SMLM to spread out a spatial connection between the DDR component and the assigned spot initiation gear, with a size of not about 50 nm.

(Ambrosio et al., 2016) DNA double stranded molecule (DSBs) trigger an immediate activation of the Dna repair (DDR) in the business, which stops the cell cycle in either G1/S or G2/M to prevent additional damage to dna. Since adult tissues include both proliferative and hibernating cells, it is probable that such two cells in the body have fundamentally distinct DDR (or G0-arrested). We investigated the differences in the entry of Downstream signaling factors and indeed the closure of DNA lesions generated by homepage DSBs in dynamically developing, S phase cells. Cells in G0 quiescence that have DSBs do not undergo repair, but instead maintain a constant amplification of the p53-pathway. However, DSBs generated in G1-synchronized or sporadically replicated cells are far more quickly repaired than all those generated in wounded G0-arrested cells, which suffer a slow repair process owing to a delay in the clearance of DNA repair parts initially attracted to DSBs.

(Furia et al., 2013) "Current methods do not allow for simultaneous quantification, high-resolution localisation, and statistically robust analysis of many parameters, which hinders the dissection of complex molecular-networks in rare cell populations. A new computational platform (Automated Microscopy for Image CytOmetry, A.M.I.CO) has been created to analyse quantitative images taken with confocal or widefield robot microscopes. We have used image-cytometry to investigate checkpoint activation in nontransformed mammary cells in response to spontaneous DNA damage. There was a link between I Ki67, a marker of proliferation, (ii) phosphorylated histone H2AX (cH2AX) and 53BP1".

II. "Materials and Methods"

2.1. "Cell Culture"

"The MCF10A cells were cultured in a medium consisting of 50% Dmem High Glucose with stable L-glutamin (DMEM) (Euroclone, Milan, Italy) and 50% Ham's F12 Medium (ThermoFisher Scientific, Waltham, MA, USA) supplemented with 5% Horse Serum, 50 ng/mL Penicillin/Streptomycin (both from Euroclone), Cholera Toxin (Merck Life Cells were cultured in 0.5% (wt/vol) gelatine in PBS on glass coverslips or in glass-bottom culture plates (MatTek, Ashland, MA, USA). At 70% confluence, 20 minutes before fixation, a final concentration of 10 M of ethidium bromide (EdU) (ThermoFisher Scientific,

Waltham, MA, USA) was added to the culture mix. For the control group, cells were fixed in 4% paraformaldehyde (wt/vol) for 10 minutes to ensure exponential development, whereas the treatment group was exposed to 5-Gy of irradiation from an X-ray machine and then fixed at the times specified".

2.2. "EdU Staining and Immunofluorescence of MCF10A Cells"

"After being fixed, MCF10A cells were washed and permeabilized with 0.1% Triton X-100 (vol/vol) in PBS for 10 minutes. According to the manufacturer's instructions, we used the Click-iT EdU Pacific Blue Imaging kit (ThermoFisher Scientific, Waltham, MA, USA) to detect EdU incorporation into DNA. This Click-iT reaction was carried out in its entirety at room temperature (RT). Samples were incubated with blocking solution (5% BSA (wt/vol) in PBS) for 30 minutes after EdU detection, and then with primary antibodies in blocking solution for 1 hour at RT. Following a 3-step PBS wash, samples were incubated with secondary antibodies for 45 minutes before being read. We used the following primary and secondary antibodies: anti-KI67 Alexa647-conjugated (558615, BD Biosciences, Franklin Lakes, NJ, USA), rabbit anti-53BP1 (ab36823, Abcam, Cambridge, UK) detected by a Pacific Orange conjugated goat anti-rabbit (P31585, ThermoFisher Scientific, Waltham, MA, USA), mouse anti-p21 (M7202, Dako, Glostrup, Denmark) (600145098, Rockland Immunochemicals, Pottstown, PA, USA). DAPI was used as a staining control for DNA. The samples were then mounted using Slowfade Gold Antifade Mountant (ThermoFisher Scientific, Waltham, MA, USA)".

2.3. "In-Situ Proximity Ligation Analysis (PLA)"

"Samples were prepared for in situ PLA using the DuoLink in situ Orange detection reagent (Sigma-Aldrich, St. Louis, MO, USA), as per the manufacturer's instructions, after EdU reaction (details below). The samples were then treated with fluorochrome-conjugated antibodies, allowing for full identification of the expression levels of the targeted molecules. Rabbit anti-53BP1 (ab36823, Abcam, Cambridge, UK), mouse anti-p53 (sc-126, Santa Cruz Biotechnologies, Dallas, TX, USA), and goat anti-p53 (DO1, Santa Cruz Biotechnologies, Dallas, TX, USA) and mouse anti-pH2AX were used as primary antibodies for PLA (613402, Biolegend, San Diego, CA, USA). Subsequent antibodies included Alexa488 anti-mouse and Alexa647 anti-rabbit or anti-goat conjugated antibodies (715-545-150 and 711-606-152, Jackson-immunoresearch, West Grove, PA, USA)".

2.4. "Automated Microscopy and Image Acquisition"

By increasing the dynamic range and minimising saturation, the best exposure period was determined for each individual fluores cence channel. Both a 60mm Plan Apo 1.4 NA (Victor Optics, Inc., Thornwood, NY) and a 60mm 1.3 NA (Olympus Corporation, Tokyo, Japan) oil-immersion objective were used for imaging (Nikon instruments, Tokyo, Japan). To capture optically sectioned multiplanar stacks, Nikon included a confocal scanhead, model A1R, on their microscope. Events were analysed and chosen using the A.M.I.CO programme based on the quantitative results of a widefield capture. With the help of the program's re-localization feature, the targeted cells were moved by transforming their picture coordinates into their real places on the stage.

III. "Result and Discussion"

3.1. "Kinetics of X-rays Irradiation Induced DNA Damage, Processing, and Cell-Cycle Arrest"

To investigate the connection between DNA-hurt demand (DDR) and cell-cycle improvement regulation, we used an image microscopy pipeline taking into consideration an electronic light elevating standard for mix. Pipeline data from seven-mix optical microscopy analysis (DNA, EdU, p53, p21, KI67, H2A.X, 53BP1) is used to create a realistic depiction of millions of cells (delegate pictures from the evaluation in

Making Figure S1). It has been shown that cells respond to DD assurance by altering their proliferation rate and expressing markers of the solid designated spot (p53 and p21) (KI67). Cells treated with the uridine necessary EdU for a short time are able to celebrate dynamic DNA affiliation, enabling for in-depth examination of the cell phone cycle disrupting impact via a "heartbeat and seek" push towards identifying early S-stage cells. The method which included the artificial nucleotide has been discarded, and the cells have been given access to fresh media without nucleotide. Thus, only cells that were really replicating their DNA during distress showed up as EdU positive, and the cell cycle progression of the illuminated cells could be tracked through G1, S, and G2M by comparing the EdU signal to the DNA stain. Since As the rapid components of this cycle were, from a macro perspective, altered by the radiation, with cells experiencing different effects depending on their stage of development when exposed to the bars. Under continuous extraordinary new development, a significant number of cells had the option to go from the G1 to the S stage, demonstrating that the G1 designated place was welcomed and preventing the transition from occuring in just a few locations. The lack of truly segregated cells in the EdU positive population at the same time point demonstrated the concurrent choice of a G2 get. Even while DNA replication was not stopped, it still had fundamental command. Consistently, under all circumstances, cells appear in the G2 phase between 3 and 6 hours, while in lit cells, it is hypothesised that 9 should 12 hours. At this moment, 24 hours after illumination, the whole population was stuck in G1 and G2 as they neared the end of the epic cell cycle.
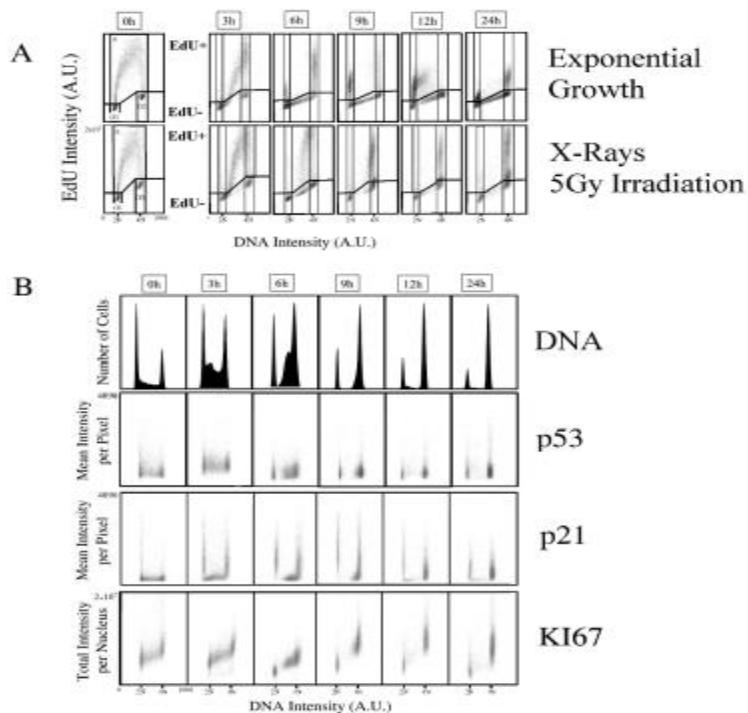

Figure 1 "Cell cycle study using image cytometry after X-ray exposure. Control and irradiated cells were subjected to a pulse of EdU, washed, and then subjected to a "chase" with fresh media (A) to analyse cell proliferation. Only reproducing cells (EdU+) at time 0 assimilate the synthetic analogue during the incubation period of 20 min. The DNA was then measured after the various populations had evolved (see Material and Methods). In (B), histograms show how DNA content is distributed over the whole cell

population (n > 5000). The expression profile of p53, p21, and KI67 in relation to DNA content at the stated time after irradiation is shown as a series of dots plots. The reported results are from a single typical experiment".
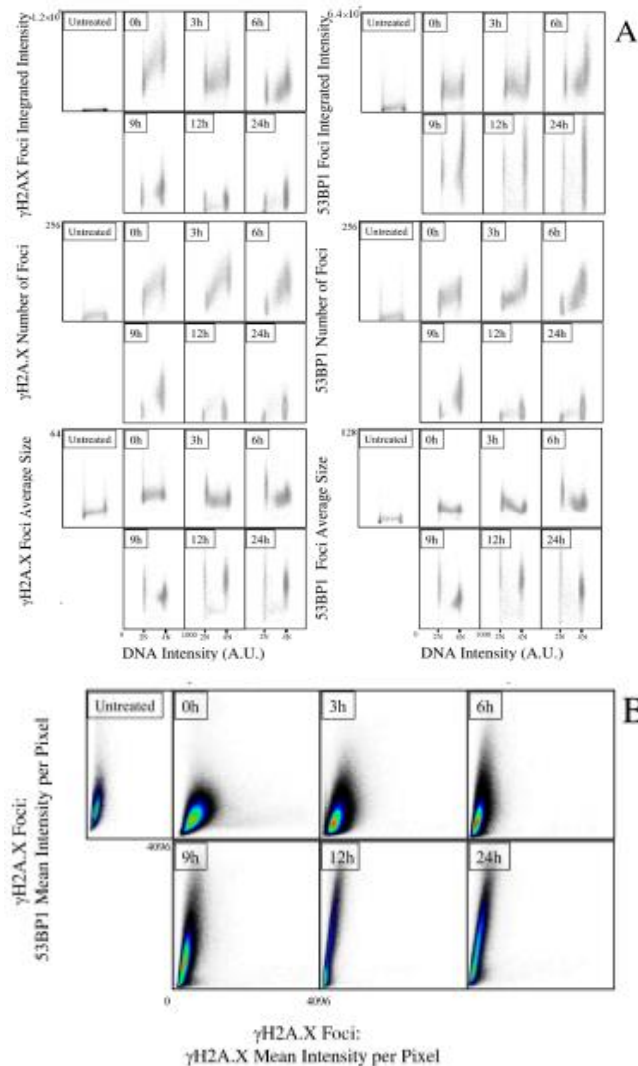

Figure 2 (A) Study of the dynamics of X-ray-induced foci formation using image cytometry. (B) statistical analysis. All of the highlighted foci (n > 105), irrespective of their cell of origin, were taken into account in the analysis. The rate of 53BP1 protein recruitment into H2A.X foci may be deduced from the distribution of the two metrics. The reported results are from a single typical experiment.

As DNA repair proceeded, the baseline level gradually dropped, eventually settling at a negligible yet sturdy 24 hours after IR receptivity. This decrease was seen not just in G1 and G2 arrested cells, but in actually replicating cells as well, indicating that continuous DNA replication and essentially equal treatment of DNA damage may be responsible for the evident regulation at the S stage end. The cellular level power of H2A.X indicated how closely the foci followed the energy, and this power decreased by an impressive factor with time.

Despite the protein's dual role in DD affirmation and fixation, the energy of 53BP1 foci exhibited a reverse direct (Figure 2, board B). It is striking that although the H2A.X foci steadily lose strength over time, after

initial recruitment, after a temporary improvement that continued throughout the whole critical cell-cycle. Acting observed for H2A.X foci seemed to be managed by increasing their number and size, lending credence to the idea that DNA damage is repaired by applying pressure. The saw scatterings painted a vivid image of the repeated sub-nuclear processes, such as the re-bounding of 53BP1 to foci that aids DD attestation and lays out DD reaction. To back up our findings, we looked at the DDR foci residents apart from the initial phone call's origin—the measurable dispersal of the signal produced by H2A. The aforementioned, indicated developments were flawlessly covered by X phosphorylation and 53BP1 enrolment. As seen by the cloud's standard allel to the X location in Figure 2 board C at 0 h, the most evil foci were ones. The vehicle of events along the bisector was triggered by the persistent enrolment caused by the DD proclamation.
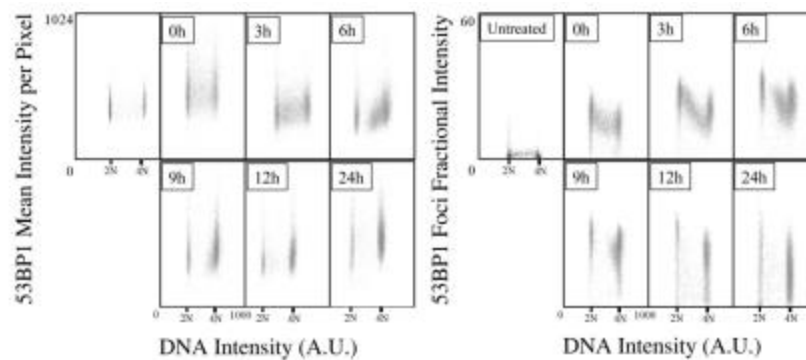

Figure 3 After being exposed to X-rays, the content and dynamics of foci of 53BP1 were studied using image cytometry. Protein concentration percentage of 53BP1 intensity localised in foci relative to total nuclear fluorescence relative to DNA concentration were analysed at the times specified.

2.2 "Kinetic High-Resolution Analysis of the Interactions among DDR and Checkpoint Molecular Networks "
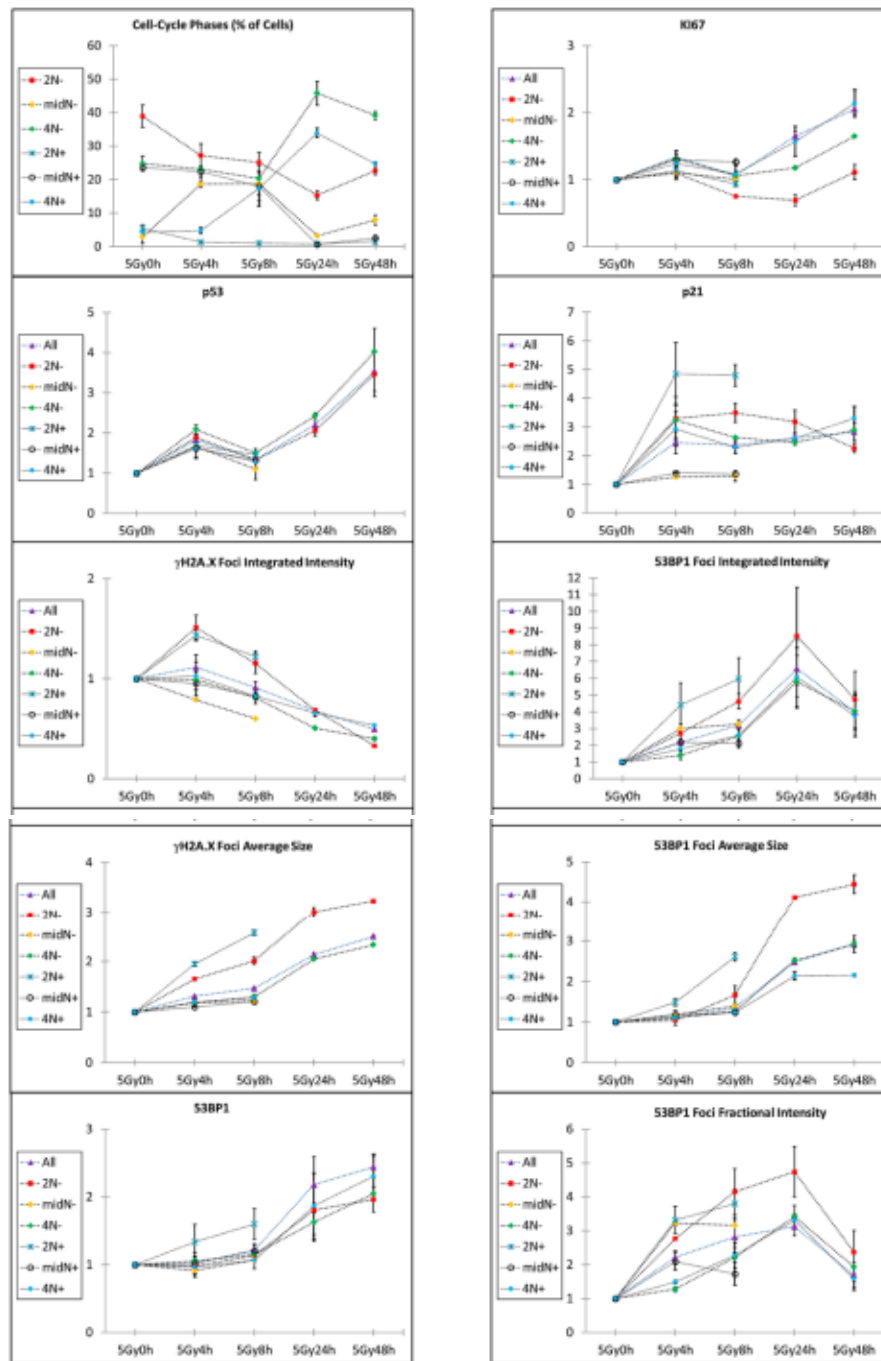
Figure 4 Analyzing the DDR-related measures and barrier protein composition in the cell cycle after 5Gy irradiation. Targeting subpopulations based on performing a statistical analysis of the stated parameters (DNA content: 2N, midN, 4N). Figure 1 depicts the geographical areas that have been accepted. Owing to the cell-cycle arrest, certain portions of the cell-cycle were not shown at subsequent time points due to a lack of sampling (number of events 500).

After illumination, the overall amount of 53BP1 protein in each cell significantly increased, as was also seen throughout the giant cell cycle. Nonetheless, its intracellular boundary was constantly shifting, in the

quantity of the protein associated with DSBs. Meanwhile, p53 was stabilised, lending credence to a theory in which 53BP1 was given to aid p53 development [14] as a means to an end express from DDR, which was drastically reduced at later time-points. The strength, quantity, and area of the IR-begun foci are communicated by an evaluation of the DD-depicting criteria tailored to a 24-hour hammering of the mischief. The confirmation and obstruction of potentially consistent endeavours is definitively required even at scattering endpoints of 200 nm, considering that some of the disparate particles demonstrates an absolute numbers (p53, p21) or a by and vast (53BP1) scattered cap in the nuclear membrane, yet constantly consequently. Using a District Ligation Evaluation, we were able to strike a sub-nuclear equilibrium while still doing extensive quantitative exploration (about 5,000 cells probed for each time point, from 104 to 106 observed foci) using a custom-built image cytometry method (PLA). In order to examine the coordinated efforts between the DDR and serous spot assisting physical party, we zoomed in on the flow unwinding differently about the peaks in p53 content. Six hours after the lighting, at the peak of the DDR's expansion, the central assessment was completed to get the gatekeepers of the genome's essential new development. Then, we waited 24-48 h post-light to distinguish the way for overseeing directing action of 53BP1 when p53 increased to design cell destiny when IR-initiated DSBs were entirely regulated.
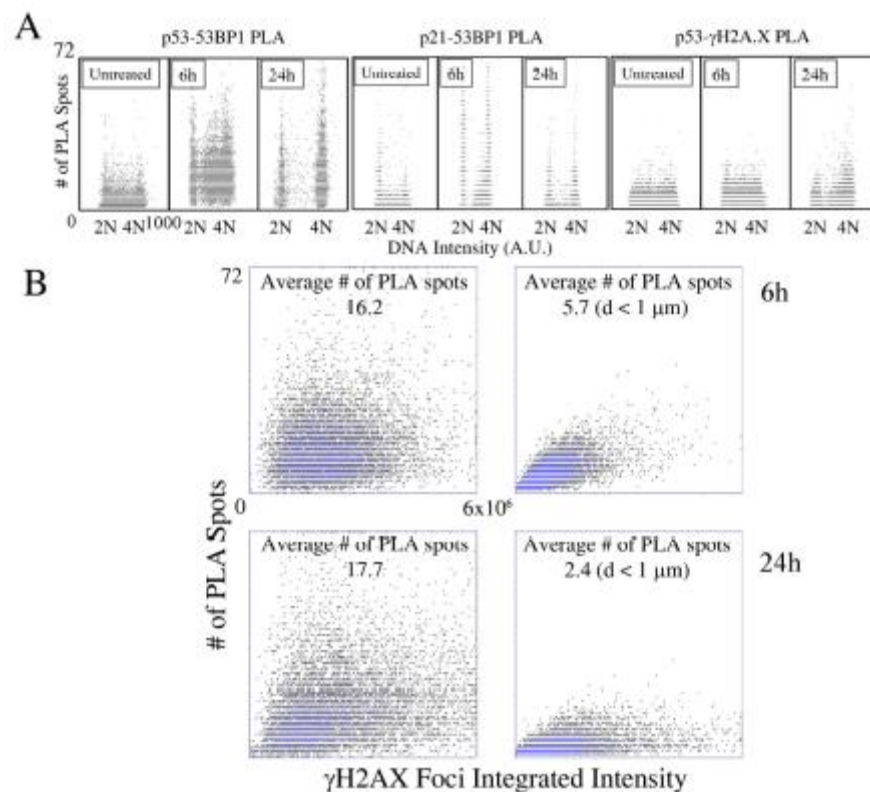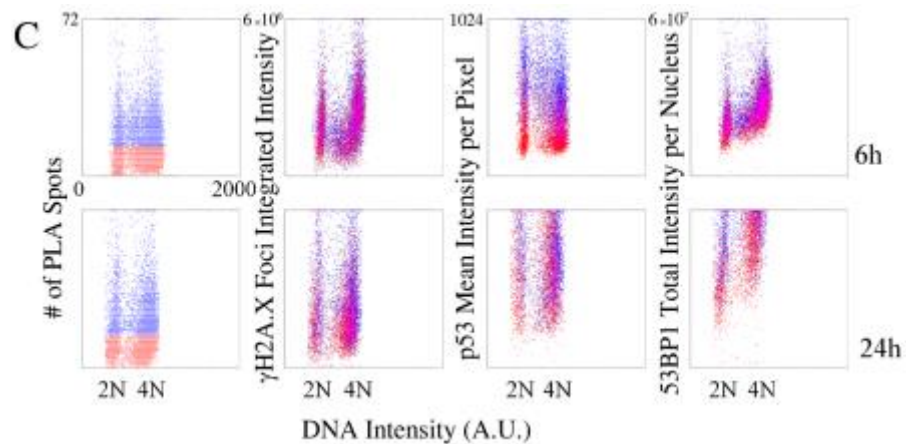
Figure 5 Protein-protein interactions observed by the Proximity Ligation Assay after X-ray irradiation and analysed by image cytometry (PLA). The number of interaction spots between the relevant proteins was measured using a PLA assay, and the bivariate distribution of DNA content is shown in (A) as a series of dot-plots. Analyzing the location of IR foci in respect to the population of PLA spots (B) (which is not dependent on the cell of origin). Only PLA locations with IR foci within 1 m were used to create the dot-plots on the right. Parameters associated with p53, 53BP1, and H2A.X are analysed (C) in relation to the strength of the 53BP1-p53 connection.
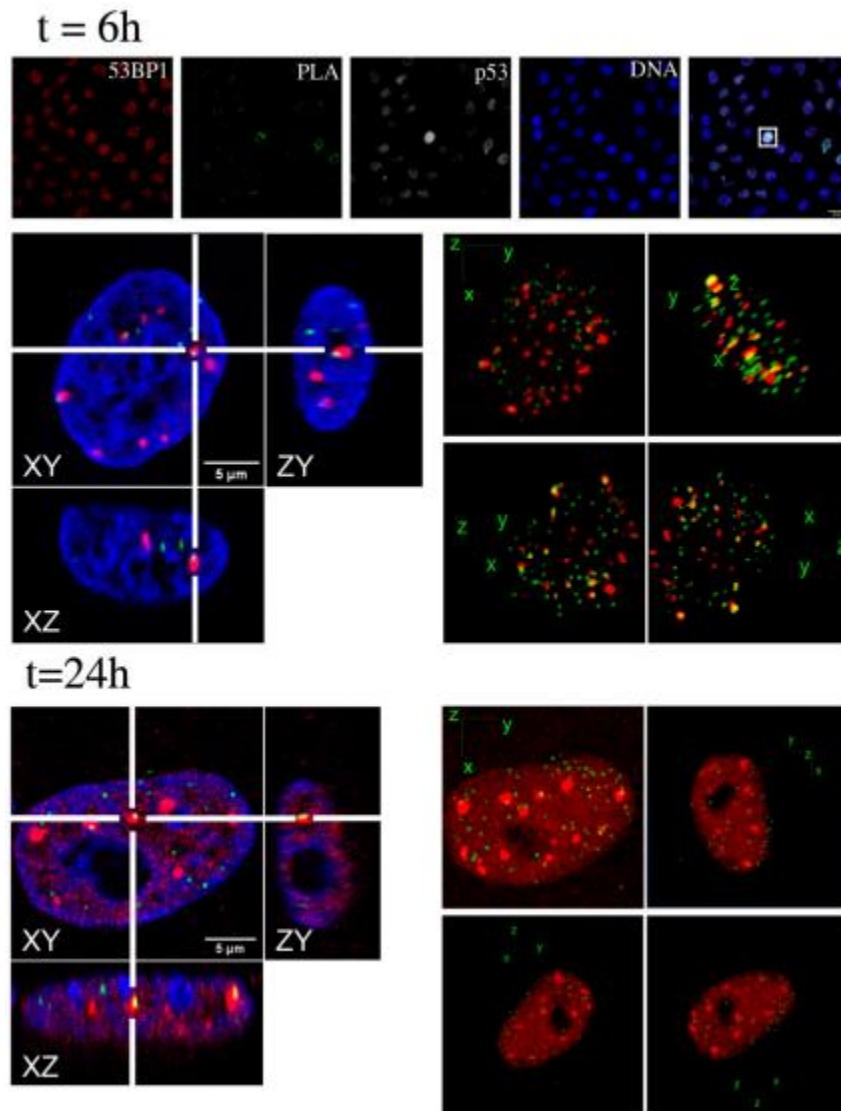
Figure 6 Imaging a possible 53BP1-p53 complex using high resolution 3D confocal microscopy. Samples labelled for the detection of 53BP1-p53 PLA spots were analysed by image cytometry to find an Eva foam k562 cell phenotype. Rearranging the cells was necessary for the optical image processing increased 3D analysis and standard and horizontal views of a selected slice (left) of a sample cell at the timings indicated.
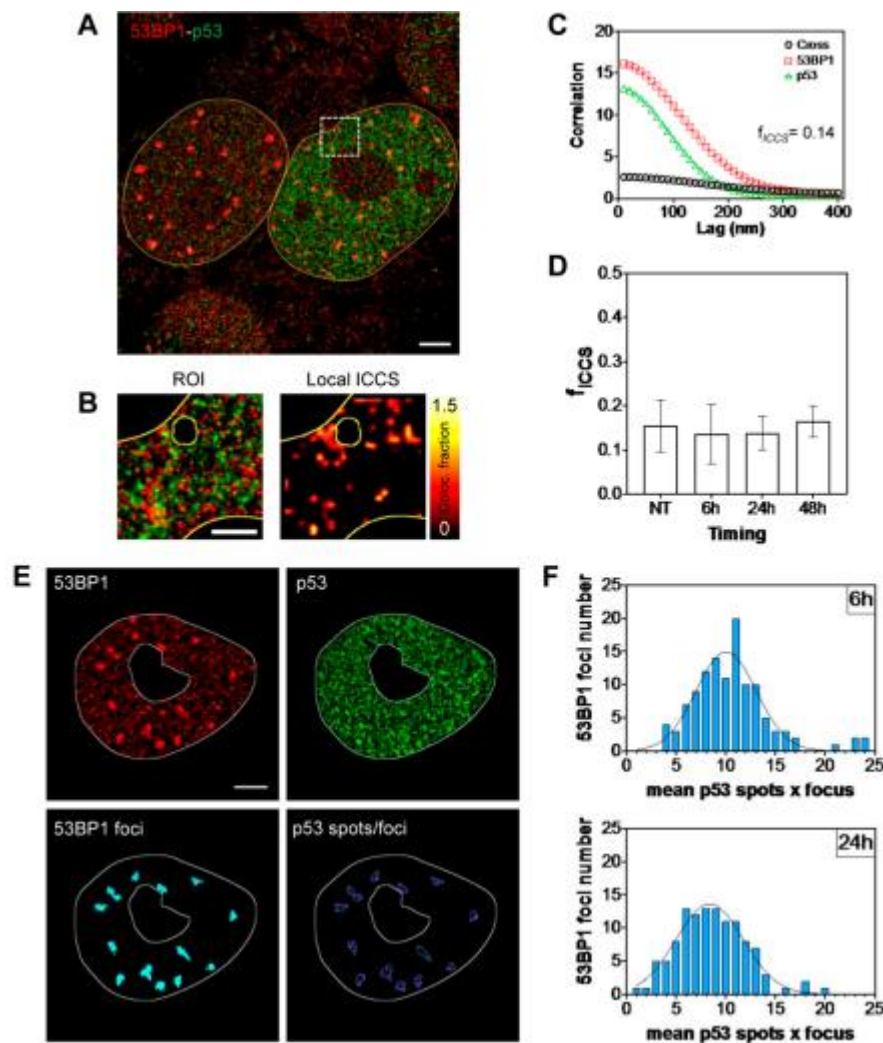
Figure 7 53BP1 and p53 mono defined by two analysis. dSTORM pictures of MCF10A nuclei labelled with 53BP1 (red) and p53 (green) are analysed (green). average standard deviation of fICCS values for 50 cells at "NT, 6 h, 24 h, and 48 h (n = 50)". The ICCS graph displays the red and green stream arrhythmia functions (circles and triangles, respectively) and the merge function (black squares) with their respective fits (solid lines). F) The frequency with which 6 h and 24 h p53 spots are seen inside 53BP1 foci. The 3 m scale bar represents one millimetre. Bar ROI represents 1 m of scale.

IV. Conclusion

The implementation of the molecular machinery focused on the validation and repair of DSBs, the pivotal dangers to the integrity of the genome, and a nearly equivalent control of both the cell biology is generally typical and requires beneficial changes in lysine residues and the development of atomic plans chosen on granted out genomic loci. With the development of fresh potential remedies contemplating formed by electrons as opposed to photon-radiation, the requirement to depict the land movement of DD created by the redirected energy occurred. In addition, because to the complex unexpected chain of events and the solidifying host environment, a multicellular perspective on the events that follow light is crucial. In spite of the fact that genomic development means has provided us with frameworks for obtaining DNA changes

back to the nucleotide sequence level and organising DNA breaks, these methods are not ideal for dealing with the ethnic diversity of cells and events that aid tumorigenesis, carbon emissions betterment, and rational response because they require single-cell objective. Stream cytometry, on the other hand, may be used to precisely link biomolecules in a single cell and do quantitative testing, but it cannot enter the actual cell itself. Fluorescence microscopy provides an unmatched opportunity for spatial resolution to address these questions. Robotic automation of image cytometry procedures for data collection and analysis might, in this manner, provide new approaches for tracking the capture of sub-atomic efforts with diffraction-limited objective. Here, we demonstrate how such a line of reasoning may be used to investigate cells' responses shortly after they have learned about photons. We shown that 53BP1 and p53, two key players in the DNA damage response (DDR), are obligated by variations in their spatiotemporal localisation inside cells, and that these improvements may be discovered using a large evident testing coexisted with a high satisfactory statistical power (up to seven fluorescence limits in the mean time). These findings not only confirmed the predicted role of the basically nebulous p53 particle near and fix of DD, but also demonstrated a rapid occupancy for the 53BP1 DDR protein in supporting the p53 activity to govern cell predetermination. Another analysis using an osteosarcoma cell model demonstrated that p53 is incorporated into H2A.X foci for a maximally liberated terminal state (U2OS). Our findings suggest the genome's guardian, p53, could play a brief role in the DNA damage response (DDR) in an unaltered cell model, thus it has been included to the rapid framework of targets allowing for further assessment to depict the phone's reaction to another kind of radiation. The vast amount of data produced is a major barrier to widespread use of massive standard image cytome effort. We enabled a system in this research to take into account the possibility of an aim that may be scaled up or down depending on the probability of the current juncture. For instance, we demonstrated how microscopy data might be used to re-keep cells of interest rapidly round of capture at the most foolish target on confined subpopulations, allowing us to go from a two- to a three-layered research. This way, we may narrow down on party photos just during particularly enlightening occasions, perhaps reducing the overall amount of data we collect.

Reference

1. Palmer SA, Smith O, Allaby RG. 2012 The blossoming of plant archaeogenetics. Ann. Anat.194, 146–156.

2. Allentoft MEet al.2012 The half-life of DNA in bone: measuring decay kinetics in 158 dated fossils.Proc. R. Soc. B 279, 4724–4733.

3. Shapiro B, Hofreiter M. 2014 A paleogenomic perspective on evolution and gene function: new insights from ancient DNA.Science343, 1236573.

4. Poinar HN et al.2006 Metagenomics to paleogenomics: large-scale sequencing of mammoth DNA.Science311, 392–394.

5. Paabo Set al.2004 Genetic analyses from ancient DNA. Annu. Rev. Genet.38, 645–679.

6. Dabney J, Meyer M, Paabo S. 2013 Ancient DNA damage.Cold Spring Harb. Perspect. Biol.5, a012567.

7. Lindahl T, Andersson A. 1972 Rate of chain breakage at apurinic sites in double-stranded deoxyribonucleic acid. Biochemistry 11, 3618–3623.

8. Lindahl T, Nyberg B. 1972 Rate of depurination of native deoxyribonucleic acid. Biochemistry 11, 3610–3618.

9. Briggs AWet al.2007 Patterns of damage in genomic DNA sequences from a Neandertal.Proc. Natl Acad. Sci. USA 104, 14 616–14 621.

10. Brotherton P, Endicott P, Sanchez JJ, Beaumont M, Barnett R, Austin J, Cooper A. 2007 Novel high-resolution characterization of ancient DNA reveals C > U-type base modification events as the sole cause of post mortem miscoding lesions. Nucleic Acids Res.35, 5717–5728.

11. Sawyer S, Krause J, Guschanski K, Savolainen V, Paabo S. 2012 Temporal patterns of nucleotide misincorporations and DNA fragmentation in ancient DNA.PLoS ONE 7, e34131.

12. Krause J, Briggs AW, Kircher M, Maricic T, Zwyns N, Derevianko A, Paabo S. 2010 A complete mtDNA genome of an early modern human from Kostenki, Russia.Curr. Biol.20, 231–236.

13. Pruvost M, Schwarz R, Correia VB, Champlot S, Braguier S, Morel N, Fernandez-Jalvo Y, Grange T, Geigl EM. 2007 Freshly excavated fossil bones are best for amplification of ancient DNA.Proc. Natl Acad. Sci. USA 104, 739–744.

14. Lindahl T. 1993 Instability and decay of the primary structure of DNA. Nature362, 709–715.

15. Yoshida K et al.2013 The rise and fall of the Phytophthora infestans lineage that triggered the Irish potato famine.eLife2, e00731.

16. Kistler L. 2012 Ancient DNA extraction from plants. Methods Mol. Biol. 840, 71–79.

17. Deagle BE, Eveson JP, Jarman SN. 2006 Quantification of damage in DNA recovered from highly degraded samples—a case study on DNA in faeces.Front. Zool.3, 11.

18. Rogers SO, Bendich AJ. 1985 Extraction of DNA from milligram amounts of fresh, herbarium and mummified plant tissues.Plant Mol. Biol.5, 69–76.

19. Martin MD et al.2013 Reconstructing genome evolution in historic samples of the Irish potato famine pathogen. Nat. Commun. 4, 2172.

20. Staats M, Erkens RH, van de Vossenberg B, Wieringa JJ, Kraaijeveld K, Stielow B, Geml J, Richardson JE, Bakker FT. 2013 Genomic treasure troves: complete genome sequencing of herbarium and insect museum specimens.PLoS ONE 8, e69189.